RESEARCH ARTICLE

An Innovative Approach to Electrical Motor Geometry Generation Using Machine Learning and Image Processing Techniques

UGUR DEMIR[1,4], GAZI AKGUN[1], MUSTAFA CANER AKUNER [1], MAJID POURKARIMI [1], OMER AKGUN [2], AND TAHIR CETIN AKINCI [3,5], (Senior Member, IEEE)

[1]Department of Mechatronics Engineering, Marmara University, 34854 Istanbul, Turkey
[2]Department of Computer Engineering, Marmara University, 34854 Istanbul, Turkey
[3]Department of Electrical Engineering, Istanbul Technical University (ITU), 34469 Istanbul, Turkey
[4]Department of Electrical and Computer Engineering, Texas A&M University, College Station, TX 77843, USA
[5]Winston Chung Global Energy Center (WCGEC), University of California at Riverside, Riverside, CA 92507, USA

Corresponding author: Tahir Cetin Akinci (tahircetin.akinci@ucr.edu)

ABSTRACT This paper presents a methodology for generating geometries for interior permanent magnet (IPM) motors in electric vehicles (EVs) through the application of artificial intelligence (AI) and image processing (IP) techniques. Due to the implementation of green agreements and policies aimed at reducing greenhouse gas emissions, EVs have become popularity. As a consequence, the improvement studies on the powertrain and battery system of EVs are focused. Especially for the powertrain, design optimization studies of e-motor have increased in the literature. One of the most widely used e-motor topologies is interior permanent magnet (IPM) motor. However, designing the IPM motor presents a challenge due to the dynamic considerations with geometric constraints. Therefore, e-motor designers encounter challenges related to determining initial geometry and the long time of the optimization process. To address these challenges, a novel approach is proposed that leverages machine learning (ML) techniques in combination with IP to generate initial geometries and design parameters for IPM motors. The proposed approach generates images of the motor geometry and extract dimensional features from the resulting images by using artificial neural networks (ANNs). The proposed method performs an analysis of the input vectors to reduce their size using techniques such as Histogram, 2D Maximum, 2D Mean, 2D Minimum, 2D Standard Deviation, and 2D Variance to enhance feature extraction. Additionally, FFT (Fast Fourier Transform) and IFFT (Inverse Fast Fourier Transform) are used to improve the neural network process in generating the image geometry. Further, the generated image geometry is improved by applying digital filtering techniques such as Log, FFT, Log+FFT, Laplacian, Sobel, and Histogram Equalization. Finally, the trained ANNs are tested to validate the results by using Ansys RMXprt and Maxwell. Eventually, the proposed method represents an innovative solution to generating initial geometries for IPM motors in EVs that satisfies desired design requirements. This approach leverages the power of AI and image processing techniques, which could lead to significant improvements in the optimization process for IPM motors, accelerate the designer's analysis process, and enhance the performance of EVs.

INDEX TERMS Artificial neural network, feature extraction, image generation, interior permanent magnet motor, machine learning, 2D filter.

I. INTRODUCTION

Electric vehicles (EVs) have become a part of our daily lives, driven largely by concerns over global warming and carbon dioxide emissions, which have now spread throughout

TABLE 1. Commonly used electric motor types [4].

Technical Properties	DC	Asynchronous	Wound Rotor Synchronous	PM Synchronous	PM Synchronous	Switched Reluctance
Field Orientation	Radial	Radial	Radial	Radial	Axial	Radial
Torque	+	-		++	++	+
Efficiency	-	-	(+/-)	++	++	+
Max. Speed	-	(+/-)		(+/-)	(+/-)	+
Cooling Performance	-	-	(+/-)	+	-	+
Field Weakening	+	+	+	(+/-)	(+/-)	(+/-)
Reliability		+		+	+	+
Economic Potential	+	++		-	(+/-)	+

the earth [1]. Transportation is responsible for over 21% of the EU's CO2 emissions, with 57% of these emissions oriented from passenger vehicles. Despite the improvement of energy efficiency, the sector's oil dependency remains over 96%. Therefore, the increasing interest of clean energy and energy savings is fueled by the demand for ecologically friendly products and fuel efficiency. The hybrid electric car vehicle (HEV) has emerged as a potential alternative for electric traction systems, and so HEV's popularity is growing in the automotive market. To minimize the carbon footprint, additional measurement processes are being developed within the framework of the Green Agreement by European Union (EU), the environmental plan set forth in line with the goal of reducing greenhouse gas emissions by 55% by 2030 and achieving carbon neutrality by 2050. The EU aims to transform the fossil fuel-based economic model entirely by extending the criteria it has established to achieve this goal to the countries with which it has commercial relations [2].

A. ELECTRIC MOTOR AS DRIVETRAIN TRACTION MODULE

EVs can be dealt with as two main varieties. These are battery electric vehicle (BEV) and hybrid electric vehicle (HEV). Two types of EVs are Battery Electric Vehicles (BEVs) and Fuel Cell Electric Vehicles (FCEVs). BEVs are powered solely by one or more electric motors. On the other hand, HEVs use both a battery to power an electric motor and an internal combustion engine that can be fueled by petroleum-based or alternative fuels [3].

Traction motors are an essential component of electric vehicles, providing the necessary torque to propel the vehicle. Electric motors can be broadly categorized as either DC or AC motors, with both types being suitable for use in electric vehicle applications. High efficiency, high instantaneous power, fast torque response, high power density, low storage, high acceleration, and robustness are all desirable characteristics for an EV motor.

The most common electric motor types are listed in Table 1. In terms of technical properties, Table 1 compare them [4]. The Permanent Magnet Synchronous Motor type is dealt with in this study considering the evaluation results in Table 1. The range extension in EVs with the same battery capacity and low range can approach 25% with the efficiency increases (6%) gained by design optimization of electric motors [5]. This means that both design and new optimization approaches are used to contribute the design of electric motors.

There are numerous optimization studies for the electric motor to satisfy desired performance requirements in the literature. Design of experiment (DoE), sequential quadratic programming, genetic algorithm, ant colony optimization, particle swarm optimization, and backtracking search algorithm are the most used optimization approaches in the literature [6], [7], [8], [9], [10].

B. AIM OF THE STUDY

Development process of EV requires the optimization of several critical technologies such as vehicle body, energy systems, management systems, and motor drive systems. Among these, the motor drive system is the most important component because it is the only source of energy for the vehicle. Therefore, the development of high-performance electric vehicle drive motors has been a focus of research for many years.

The critical aspect of design of a drive motor is the parameter matching between geometric design and desired performance. Computer-aided design tools are used to perform extensive electromagnetic, electromechanical, and thermal analyses of electric motors. A virtual prototype of the motor is modeled, and design software solutions determine the electrical, magnetic, mechanical, and thermal values results of various types of electric motors. This process enables manufacturers to evaluate the best motor design before production.

Electrical machine manufacturers seek to create the best and cost-effective motor design and bring them to the market quickly. To analyze and design the performance of electric motor using simulation software may enhance market competitiveness. The simulation performance of electric motors can be considered as accuracy and calculation time.

The computational and numerical simulation approaches are used to calculate the performance of electric motors. These approaches include classic closed-form analysis, clustered parameter models based on definitions obtained from finite element analysis, and non-linear time-based finite element analysis. Each method has advantages and disadvantages, but all of them provide valuable insights into electric motor performance.

The development of high-performance electric vehicle drive motors using advanced computer-aided design tools and simulation software is a critical step in achieving this goal. Therefore, this study focuses on avoiding the iterative optimization process to reduce the long simulation time by using neural network. In this way, the challenge the creating the initial design of geometry can be overcame for minimization of the development process.

For example, a 2D Geometric FEM Analysis of E-motor may take 200 minutes considering the average 200 iterations depends on the computation speed of the workstation. On the other hand, the duration of a 2D Geometric FEM Analysis of E-motor in the case of successful initial geometry generated by NN may reduce up to 5 iterations, therefore the analysis may take 5+15 (NN training) minutes. And this achievement provides the designer more time to build the optimal e-motor.

C. DESIGN OPTIMIZATION STUDIES FOR E-MOTOR

There are a lot of design optimization studies for e-motor in the literature. In summary, in these studies copper losses, state of charge, damage analysis, efficiency, power consumption, heat transfer analysis, core losses, fuel consumption, power losses, current density, rated power, torque density, iron losses, torque ripple, winding temperature and driver losses are investigated in terms of the performance metric such as acceleration, hill start, over loading, normal cruise, regenerative breaking, speed variation. And geometric e-motor design parameters are tried to be optimized by using the algorithm such as Frequency Cubic, Sequential Surrogate Optimizer, Genetic Algorithm, Sequential Quadratic Programming, System-Based Minimization, Machine-Based Minimization Algorithms, Bi-Objective Optimization, Multi-Objective Design Optimization, Multi-Objective Genetic Algorithm, Multi-Objective Sequential Optimization Method, Root-Mean-Square Error, Kriging model using NSGA-II, Central Composite Design, Loss-Minimization Algorithm, Differential Evolution Algorithm, Base Point Optimization, Particle Swarm Optimization, Design of Experiment and Non-dominated Sorting Genetic Algorithm [11], [12], [13], [14], [15], [16], [17], [18], [19], [20], [21], [22], [23], [24], [25], [26], [27], [28], [29], [30], [31], [32], [33], [34], [35], [36], [37], [38], [39], [40]. All the
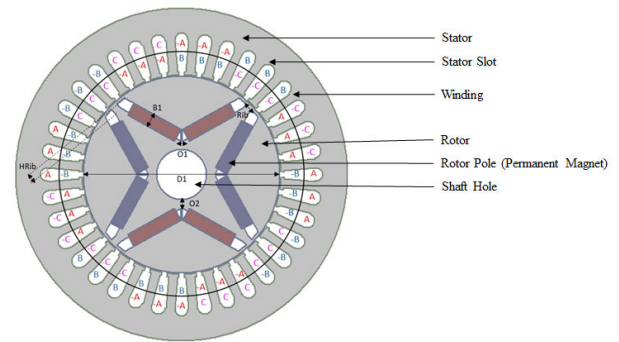

FIGURE 1. IPM structure.

algorithms mentioned here are techniques that are used for e-motor analysis, such as the numerical or iterative (finite element) method, to obtain results by running iteratively on algorithms. In addition to the long calculation times of methods such as finite elements, the optimization process takes a long time with iterative optimization algorithms. The important point here is that this optimization process basically depends on the initial geometry. If it can be started with a suitable initial geometry, optimization processes can be shortened considerably. Here, the main purpose of this study is to derive the most suitable initial geometry.

D. CONTRIBUTION

Electric motor design is geometry depended process. Therefore, the process of geometry generation and calculation is crucial to improve efficiency and desired performance of the electric motor. For the design process, topology optimization has a significant role in recent years as it enables the discovery of new structures during the conceptual design phase. Additionally, deep learning can accelerate topology optimization using evolutionary algorithms, leading to faster fitness evaluation without the need for time-consuming finite element methods. Topology optimization offers a groundbreaking framework for creating high-performance electric motors that may not be achievable through traditional engineering methods [41], [42], [43].

Artificial Neural Networks (ANNs) are utilized for classification and regression tasks, extracting features from input images automatically. It means that ANNs can extract torque performance information from cross-sectional images of interior permanent magnet (IPM) motors. To perform the recognition of the pattern of IPM motor, ANNs need training data that includes labeled performance data and cross-sectional images geometry of the e-motor.

Deep Learning, or Deep Neural Networks (DNNs), refers to multi-layer ANNs. This approach has been recognized as one of the most powerful tools in recent years and is widely utilized in the literature due to its ability to handle vast amounts of data and creating meaningful results [44].

It is aimed to contribute to the literature with a method developed with neural network approach and image
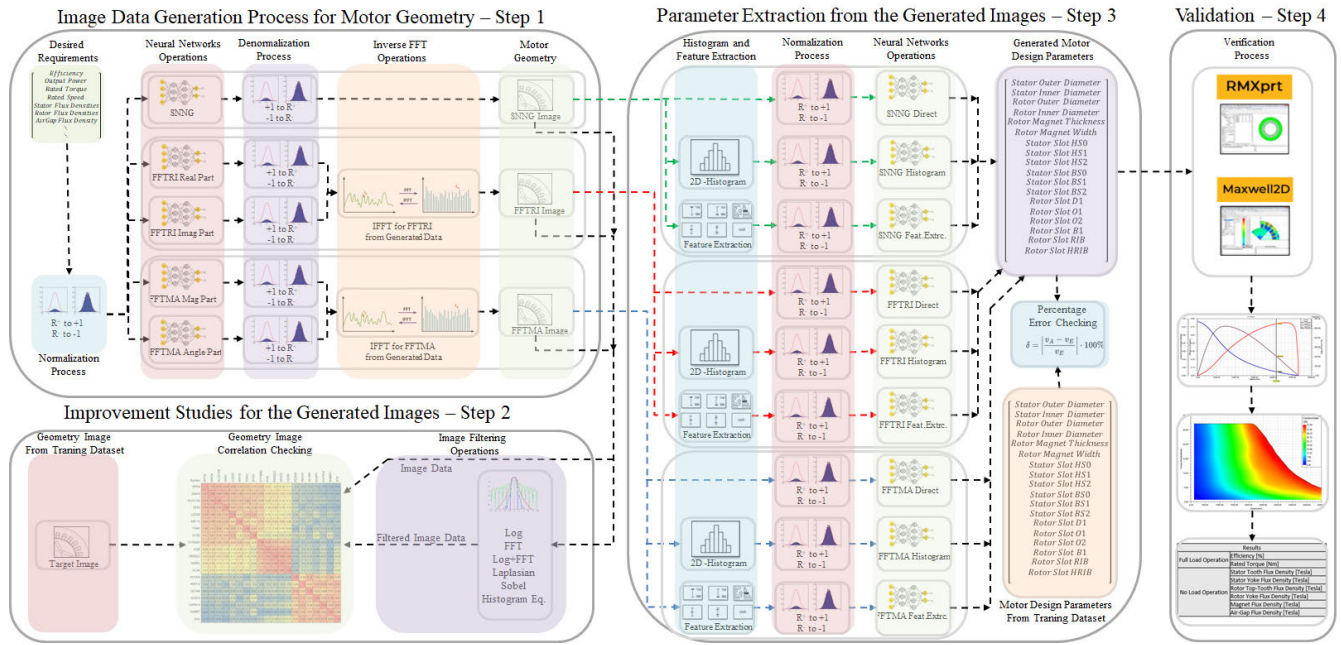
FIGURE 2. The process steps of the methodology.

processing techniques in order to derive the initial e-motor geometry as an image by reducing the iterative optimization times and to extract the design parameters with geometric dimensioning.

II. IPM STRUCTURE AND OPERATION PRINCIPLE

The widespread usage of electric powertrain is replacing traditional internal combustion engines to reduce fossil fuel consumption, exhaust emissions, and improve vehicle efficiency and performance [45], [46], [47], [48]. One of the primary technologies contributing to this transformation is the electric traction motor, known for its high-power density, wide speed range, and efficiency [49], [50]. AC traction machines, which are more efficient than DC traction machines, dominate the market due to enhanced power electronics and contemporary controls. Both synchronous and asynchronous AC machines are used in commercially available electric vehicles, with asynchronous machines being a more established technology with lower costs and better controllability, but with increased rotor copper losses due to conductors on the rotor, leading to higher cooling requirements and lower overall operating efficiency compared to permanent magnet synchronous machines (PMSM) [51], [52].

In the past two decades, interior permanent magnet (IPM) motor have undergone significant development, and have become popular in the automotive sector. IPM motors are widely employed in automotive and other servo drives due to their superior advantages such as high efficiency, high torque density, high power factor, high power density, and wide speed range operation [53], [54], [55]. The geometric structure of an IPM motor is shown in Fig. 1. An IPM motor has a permanent magnet structure which is placed in the

rotor, which reduces the reluctance torque and chance of magnet stripping by centrifugal force, and can be embedded in various constructions, making it easier to manufacture and more efficient than surface permanent magnets. IPM motors are also compatible and easy to replace with standard asynchronous motors of the same size, with the highest efficiency level of all electric motor types, synchronous rotation speed, no slip, precise speed control, and use of a standard inverter.

The magnet position is optimal, leading to minimal losses compared to standard asynchronous motors, with less loss in the rotor, and other benefits such as the ability to change balls without removing the rotor, less fan noise with smaller fans, and energy savings [56]. In the literature, there are a lot of studies for the IPM motor to analyze its performance and to understand the dynamical behaviour. It has been observed that the geometric design parameters of the IPM motor are associated with the performance outputs in order to provide the desired requirements for the powertrain of EV.

III. METHODOLOGY

In this study, artificial neural networks, filter techniques, and machine learning algorithms are used to predict the geometry and extract features of the targeted electric motor. Fig. 2 illustrates the generalized process steps.

A. THE OPERATING PRINCIPLE

As can be seen from Fig. 2, the process includes 4 steps. Here, it is attempted to generate the image of the motor geometry that satisfies the desired design requirements. Then, the design metric (geometric dimensions) of the motor geometry is tried to be extracted.

1) STEP 1

In this step, the image of the motor geometry is generated. The design requirements such as desired motor efficiency, motor power, rated speed, rated torque, stator, rotor, and air gap flux density constraints are taken as a vector matrix in a Matlab©environment. Then, these data are normalized. The normalized vector is transmitted as input to 5 different neural networks (NN) so that the trained neural networks generate an output matrix. Here, the block with one neural network structure is denoted SNNG. And it is intended to generate directly the image of the motor geometry. Since it is known that 2-dimensional direct and inverse Fourier transforms have important properties in the processing of image matrices, it is also desired to benefit from the Fourier transform in this section [57]. Therefore, two different neural networks for FFTRI Real Part and FFTRI Imag Part are used to evaluate the obtained real and imaginary parts after the Fourier transform, and two different neural networks for FFTMA Mag Part and FFTMA Angle Part neural networks are used to evaluate the obtained magnitude and angle parts after the Fourier transform. The generated output matrices from 5 different NNs are denormalized, and each parameter is returned to its numerical magnitudes. Then, FFTRI Real Part and FFTRI Imag Part are transmitted to the inverse FFT (IFFT) process to compose the image of the motor geometry. Similarly, FFTRI Mag Part and FFTRI Angle Part are transmitted to the inverse FFT (IFFT) process to compose the image of the motor geometry. Thus, 3 generated images of the motor geometry from SNNG, FFTRI, and FFTMA neural networks are obtained.

2) STEP 2

Here, some filter techniques such as Log, FFT, Log+FFT, Laplacian, Sobel and Histogram Equalization are used to improve the noise on the obtained images and to increase the correlation to the motor geometry matrices used as training data. Then, the used image of the motor geometry as training data, the filtered and unfiltered images are analyzed and evaluated according to the correlation results. Logarithmic transform is an image enhancement technique which is used to correct the intensity distribution in the image matrix generated by SNNG. The logarithmic transformation given in (1) is used to increase the pattern generated by SNNG to a visible level. Where S is the output image, c is the constant and r is the input image.

$$S = c\log(1 + r) \qquad (1)$$

The histogram equalization is a histogram transformation method used to transform the intensity distribution into a shape. Here, when the cumulative distribution function has (cdf) given in equation 2 is applied on the image histogram, the histogram distribution of the image is to be uniform and as in (2) [58].

$$p_S(s) = \frac{1}{L-1} \qquad (2)$$

This technique ensures that the intensity distribution in the image is evenly distributed between full dark and full light, and standardizes the color contrast.

$$T(r) = (L-1)\int_0^r p(r)\,\omega d\omega \qquad (3)$$

In (3), $T(r)$ is the cdf applied image matrix, L is the intensity resolution of the image and $p(r)$ is the histogram distribution vector of the input image.

The Laplacian is the divergence of the vector obtained by taking the gradient of a scalar field. It is applied in both spaces of the image matrix, allowing discontinuities to be emphasized, and continuous points are suppressed. As can be seen in (4), Laplacian, which is calculated by taking the second-order discrete-time derivative in both spaces, is a useful method for finding the edges in the image.

$$\nabla^2 f = \frac{\partial^2 f}{\partial x^2} + \frac{\partial^2 f}{\partial y^2}$$
$$\frac{\partial^2 f}{\partial x^2} = f(x+1,y) + f(x-1,y) - 2f(x,y)$$
$$\frac{\partial^2 f}{\partial y^2} = f(x,y+1) + f(x,y-1) - 2f(x,y) \qquad (4)$$

The Sobel filter provides estimating discontinuities by convoluting the kernels from (5) with the image matrix, this approach gives directional gradient matrices as well as amplitude and angle matrices [59].

$$G_x = \begin{vmatrix} -1 & 0 & 1 \\ -2 & 0 & 2 \\ -1 & 0 & 1 \end{vmatrix} \quad G_y = \begin{vmatrix} -1 & -2 & -1 \\ 0 & 0 & 0 \\ 1 & 2 & 1 \end{vmatrix}$$
$$M(x,y) \approx |G_x| + |G_y|$$
$$A(x,y) = atan2\left(\frac{I \star G_x}{I \star G_y}\right) \qquad (5)$$

Here $G_x, G_y, M(x,y), I, A(x,y)$ and $'\star'$ represent the sobel kernels, magnitude, the image matrix, the edge angle matrix and the convolution operation, respectively.

The Fourier transform is the process of transforming the image from the spatial domain to the frequency domain. With this process, the image can be easily filtered by separating its frequency components. The discrete-time Fourier transform equation is given in (6) [60]. FFT (Fast Fourier Transform) method is used in this study.

$$F(\mu,v) = \sum_{x=0}^{M-1}\sum_{y=0}^{N-1} f(x,y)e^{-j2\pi(\mu x/M + vy/N)}$$
$$\mu = 0,1,2,\ldots, M-1; v = 0,1,2,\ldots, N-1; \qquad (6)$$

where f represent the image matrix. M and N are the spatial pixel numbers of the image. μ and v are the frequency variables.
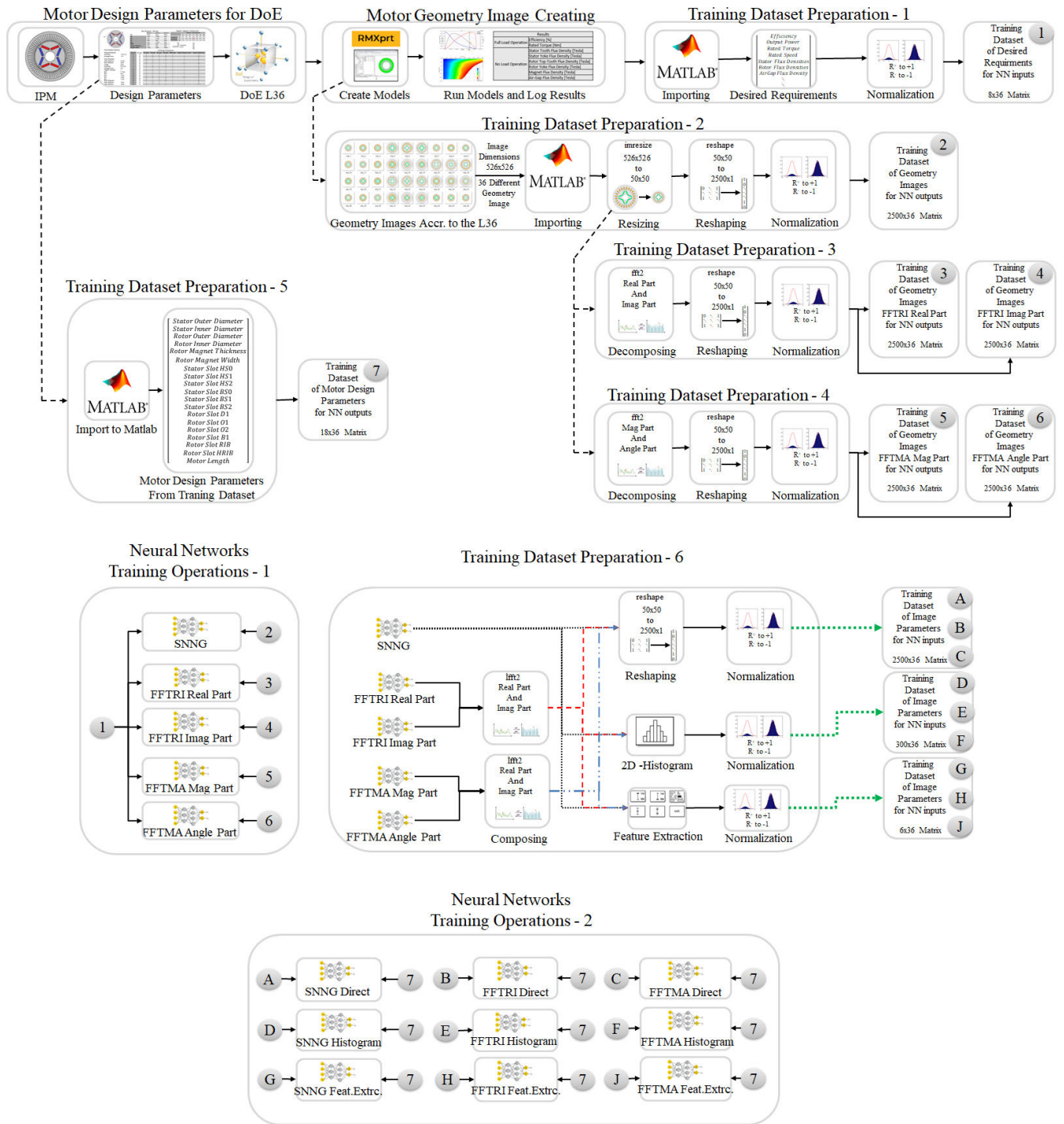
FIGURE 3. Dataset preparing and model training processes.

3) STEP 3

Here, the design parameters of the generated images of the motor geometry are extracted. In order to extract the design parameters, it is considered to analyze the results comparatively by evaluating 3 different geometry images (SNNG Image, FFTRI Image, and FFTMA Image) in 3 different categories. These 3 different categories consist of Direct, Histogram, and Feat.Extrc. The Direct is used the generated image geometry data without any process. The Histogram is used by considering Histogram data. And the Feat.Extrc. is used Feature Extraction data. The reason for this way is to observe the performance of NN in different matrix sizes,

because of 2500 × 1 matrix size for Direct operation, 300 × 1 matrix size for Histogram, and 6 × 1 matrix size for Feat.Extrc are dealt with.

Considering these combinations, 9 different NNs are created. These consists of NNs with SNNG Direct, FFTRI Direct, FFTMA Direct, SNNG Histogram, FFTRI Histogram, FFTMA Histogram, SNNG Feat.Extrc., FFTRI Feat.Extrc. and FFTMA Feat.Extrc. Input data coming to the inputs of these neural networks is applied to the input of NN by normalizing for SNNG Direct, and FFTRI Direct, FFTMA Direct. For the SNNG Histogram, FFTRI Histogram and FFTMA Histogram, the generated image of the motor geometry is applied to the NN inputs after the Histogram algorithm (Equation 6) and then normalized [61]. On the other hand, For SNNG Feat.Extrc., FFTRI Feat.Extrc. and FFTMA Feat.Extrc., the generated image of the motor geometry is applied to the NN inputs after the Feature Extraction algorithm and then normalized.

Due to the nonlinear structure of the ANN algorithm, the relationships on the input information must be dimensioned in order to make a successful classification. The defined dimensions by different mathematical relations create a frame in which neural networks can solve the linear classification problem. The selected features increase the success of ANN by carrying the problem to a multidimensional space. In this study, 2D Maximum, 2D Mean, 2D Minimum, 2D Standard Deviation and 2D Variance attributes are dealt with the histogram of the image and its components in the frequency space [62], [63].

These statistical parameters are used as auxiliary tools to implement processing results that increase linear classification such as histogram and frequency conversion. The maximum, average, and minimum information in the frequency domain and histogram area, which are formed with certain framing coefficients in the spatial domain, give information about the rank statistics, and the standard deviation and variance give information about the distribution statistics. The motor design parameters related to stator and rotor inner and outer diameters, stator and rotor slot geometries and magnet dimensions are extracted as an output of NNs. The obtained motor design parameters are compared with the motor design parameters used as training data and the percentage errors are analyzed and evaluated.

$$p\left(r_{k}\right)=\frac{n_{k}}{MN} \tag{7}$$

In (7), $p\left(r_{k}\right)$ is the probability density function (histogram distribution) of the image matrix. MN is the pixel number of the image, and n_{k} is the frequency of the intensity value in the image matrix.

4) STEP 4
Here, the extraxted motor design parameters are modeled in Ansys RMXPrt and Maxwell Environment. Then, the model are compared with the desired design parameters in Step 1 and analyzed in various scenarios.

B. THE TRAINING PROCESS FOR NNs
The preparation of data sets for the neural networks shown in Fig. 2 includes various steps. The detailed process steps are given in Fig. 3. As can be seen from Fig. 3, the preparation of training sets consists of gradual and various steps. These steps are carried out by extracting the motor design parameters for the design of experiments (DoE), creating the image of the motor geometry, preparing the training data and performing the training processes.

Design of experiment (DoE) are used to create the training data set. Here, 18 motor design parameters (for minimum, average and maximum values of the parameters) and 8 factors are considered to run DoE. To perform DoE, L36 for 18 motor design parameters and 3 Levels is determined as orthogonal array. Therefore, 36 × 1 different motor geometry, design parameters 36 × 18 and performance results 36 × 8 are created as training data set.

Basically, this study consists of parameter fitting operation therefore neural network structure is determined for fitting process. All NN structures has 2 layers which are hidden and output layers. The neuron number in the output layer of all NNS is depended with the desired output vector (2500). However, the neuron number in hidden layer of all NNs is optimized for input (8) and output (2500) vector. Here in the 1st step (image generation) shown in Fig.2, all NN structure have same input and output neurons. These neuron number in hidden layer are optimized by Box Behnken Design (BBD) which provides experimental results. In BBD, 10, 100 and 1000 neurons in hidden layer is run and resulting of the linear regression an optimal neuron number are calculated as 275 in hidden layer to avoid the long calculation process. And the output layer has already 2500 neuron due to the expected motor geometry (50 × 50). On the other hand, in the 3rd step (parameter extraction) shown in Fig.2, there are basically 3 different input vector as Direct (2500 × 1), 2D Histogram (300 × 1), and Feature Extraction (6 × 1). and there is one type of output vector as 18 × 1, therefore all NNs here have 18 neurons. Similarly, the neuron number in hidden layer are optimized by Box Behnken Design (BBD) which provides experimental results. In BBD, 10, 100 and 1000 neurons in hidden layer is run and resulting of the linear regression an optimal neuron number are calculated as 225 in hidden layer. During the BBD, all assessments are performed considering the results of MSE (Mean Squared Error) and R (Regression).

1) MOTOR DESIGN PARAMETERS FOR DoE
Here, the determining of the design parameters for the IPM and DoE scenarios are dealt with. Considering the parameters in the stator and rotor geometries, 18 parameters are taken into account. These are Stator Outer Diameter SOD and Stator Inner Diameter SID, Stator Slot S_HS0, Stator Slot S_HS1, Stator Slot S_HS2, Stator Slot S_BS0, Stator Slot S_BS1, Stator Slot S_BS2, Rotor Outer ROD and Inner Diameter RID, Rotor R_D1, Rotor R_O1, Rotor R_O2, Rotor R_B1, Rotor R_RIB is Rotor R_HRIB, Magnet Thickness

TABLE 2. Training results and features for NNs.

| NN (Neural Networks)	Input	Output	Hidden Layer	Output Layer	Training Algorithm	MSE	Regression
SNNG	8	2500	tansig	purelin	Scaled Conjugate Gradient	0.013393	0.942574
FFTRI Real Part	8	2500	tansig	purelin	Scaled Conjugate Gradient	2.32E-06	0.989034
FFTRI Imag Part	8	2500	tansig	purelin	Scaled Conjugate Gradient	0.001196	0.956307
FFTMA Mag Part	8	2500	tansig	purelin	Scaled Conjugate Gradient	2.19E-07	0.989094
FFTMA Angle Part	8	2500	tansig	purelin	Scaled Conjugate Gradient	0.004029	0.992679
SNNG Direct	2500	18	tansig	purelin	Scaled Conjugate Gradient	28.87191	0.9808
FFTRI Direct	2500	18	tansig	purelin	Scaled Conjugate Gradient	0.452252	0.999704
FFTMA Direct	2500	18	tansig	purelin	Scaled Conjugate Gradient	0.002722	0.99998
SNNG Histogram	300	18	tansig	purelin	Scaled Conjugate Gradient	0.020562	0.926114
FFTRI Histogram	300	18	tansig	purelin	Scaled Conjugate Gradient	0.019321	0.906228
FFTMA Histogram	300	18	tansig	purelin	Scaled Conjugate Gradient	0.002321	0.955964
SNNG Feat.Extrc.	6	18	tansig	purelin	Levenberg-Marquardt	4.58E-21	0.99998
FFTRI Feat.Extrc.	6	18	tansig	purelin	Levenberg-Marquardt	2.83E-21	0.99998
FFTMA Feat.Extrc.	6	18	tansig	purelin	Levenberg-Marquardt	3.21E-28	0.99998
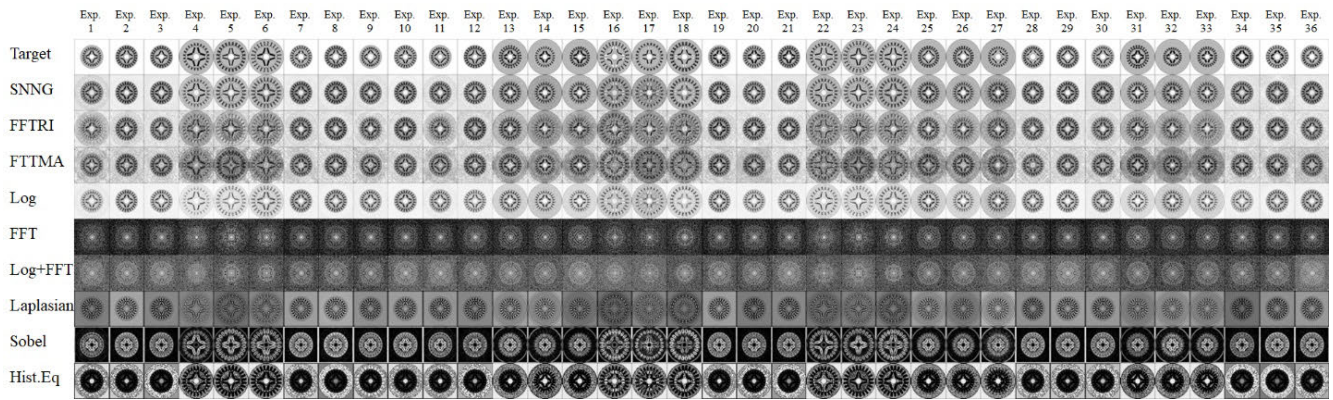
FIGURE 4. Generated motor geometries from nns and training targets.

R_MT and Width R_MW. When these parameters are considered as a 3-level orthogonal array, the L36 matrix is chosen. The experimental parameters are prepared according to the scenarios in L36.

2) MOTOR GEOMETRY IMAGE CREATING

36 different motor models for L36 are modeled and analyzed in Ansys RMXPrt and the results are logged.

3) TRAINING DATASET PREPARATION—1

The results of the motor models created in Ansys RMXPrt are imported to the Matlab©working environment and 8 × 36 matrix is created for Efficiency [%], Rated Torque [Nm], Stator Tooth Flux Density [Tesla], Stator Yoke Flux Density [Tesla], Rotor Top-Tooth Flux Density [Tesla], Rotor Yoke Flux Density [Tesla], Magnet Flux Density [Tesla] and Air-Gap Flux Density [Tesla]. Then, this matrix is normalized and saved as data on the NN input side as the desired motor design requirements.

4) TRAINING DATASET PREPARATION—2

The images of the motor models created in Ansys RMXPrt are saved as JPEG format and imported to the Matlab working environment. The images of the motor geometry consist of a 526 × 526×3 dimensional matrix.

Considering the Workstations in our laboratory, it is preferred to the data reduction, as it would increase the performance of the process. Then, the RGB images are transformed to Gray format and so the dimension of the matrix is 526 × 526. Then, the 526 × 526 sized matrices are resized and transformed to 50 × 50 sized matrices. For NN training, 2500 × 1 dataset is prepared by transforming the 50 × 50 matrix into a vector matrix. Then, it is passed through the normalization process and saved as data on the NN output side as the images of the motor geometry.

5) TRAINING DATASET PREPARATION—3

It decomposes the 50 × 50 matrices obtained in the previous step with FFT. As a result of the decompose process, 2500 × 1

TABLE 3. L36 experiments (in millimeter).

Exp.No	SOD	SID	ROD	RID	R_MT	R_MW	S_HS0	S_HS1	S_HS2	S_BS0	S_BS1	S_BS2	R_D1	R_O1	R_O2	R_B1	R_RIB	R_HRIB
1	78	49	48	17	3	26	0.35	0.65	5.3	1.6	3.7	5	46	2	2	2.5	2	2
2	78	49	48	17	3	26	0.5	1	8.2	2.5	5.6	7.6	46	3	3	4	3	3
3	78	49	48	17	3	26	0.5	1	8.2	2.5	5.6	7.6	46	2	2	2.5	2	2
4	120	75	74	20	5	40	0.35	0.65	5.3	1.6	5.6	7.6	72	3	4	5.5	4	4
5	120	75	74	20	3	40	0.5	1	8.2	2.5	7.5	10.2	72	4	2	2.5	2	2
6	120	75	74	20	5	40	0.65	1.35	11	3.4	3.7	5	72	2	3	4	3	3
7	78	49	48	20	3	26	0.35	0.65	8.2	3.4	3.7	7.6	46	4	2	4	3	4
8	78	49	48	20	3	26	0.5	1	8.2	1.6	5.6	7.6	46	4	2	4	3	2
9	78	49	48	20	3	26	0.65	1.35	5.3	2.5	5.6	5	46	3	4	2.5	2	2
10	78	49	48	17	3	26	0.35	0.65	8.2	2.5	3.7	7.6	46	4	3	2.5	4	2
11	78	49	48	17	3	26	0.5	1	5.3	3.4	5.6	5	46	2	4	4	2	4
12	78	49	48	17	3	26	0.65	1.35	8.2	1.6	5.6	7.6	46	2	2	4	2	2
13	120	49	48	17	5	26	0.35	1	11	1.6	5.6	7.6	46	4	3	4	3	3
14	120	49	48	17	5	26	0.5	1.35	5.3	2.5	3.7	7.6	46	2	2	4	4	4
15	120	49	48	17	5	26	0.65	0.65	8.2	3.4	5.6	5	46	3	3	4	4	2
16	120	75	74	20	3	26	0.35	1	11	2.5	3.7	5	72	3	4	5.5	3	2
17	120	75	74	20	3	26	0.5	1.35	5.3	3.4	5.6	7.6	72	4	2	2.5	4	3
18	120	75	74	20	3	26	0.65	0.65	8.2	1.6	7.5	10.2	72	2	3	4	2	4
19	78	49	48	17	5	26	0.35	1	5.3	3.4	5.6	7.6	46	4	3	4	4	2
20	78	49	48	17	5	26	0.5	1.35	8.2	1.6	3.7	5	46	4	3	4	4	2
21	78	49	48	17	5	26	0.65	0.65	8.2	2.5	5.6	7.6	46	2	2	4	3	2
22	120	75	74	17	3	40	0.35	1	8.2	3.4	7.5	5	72	2	2	5.5	4	3
23	120	75	74	17	3	40	0.5	1.35	11	1.6	3.7	7.6	72	3	3	2.5	2	4
24	120	75	74	17	3	40	0.65	0.65	5.3	2.5	5.6	10.2	72	4	4	4	3	2
25	120	49	48	20	3	26	0.35	1.35	8.2	1.6	5.6	7.6	46	2	4	2.5	3	3
26	120	49	48	20	3	26	0.5	0.65	11	2.5	5.6	5	46	3	2	4	4	4
27	120	49	48	20	3	26	0.65	1	5.3	3.4	3.7	7.6	46	4	3	5.5	2	2
28	78	49	48	20	3	26	0.35	1.35	8.2	2.5	5.6	5	46	4	3	5.5	2	4
29	78	49	48	20	3	26	0.5	0.65	8.2	3.4	5.6	7.6	46	2	4	2.5	3	2
30	78	49	48	20	3	26	0.65	1	5.3	1.6	3.7	7.6	46	3	2	4	4	3
31	120	49	48	17	5	26	0.35	1.35	11	3.4	5.6	7.6	46	3	2	4	2	2
32	120	49	48	17	5	26	0.5	0.65	5.3	1.6	5.6	5	46	4	3	4	3	3
33	120	49	48	17	5	26	0.65	1	8.2	1.6	5.6	5	46	4	2	4	4	4
34	78	49	48	20	5	26	0.35	1.35	5.3	2.5	5.6	7.6	46	2	3	3	4	2
35	78	49	48	20	5	26	0.5	0.65	8.2	3.4	3.7	7.6	46	3	4	4	2	3
36	78	49	48	20	3	26	0.65	1	8.2	1.6	5.6	5	46	4	2	2.5	3	4

TABLE 4. Correlation results for NNs.

NNs	SNNG	FFTRI	FFTMA	Log	FFT	Log+FFT	Laplasian	Sobel	Hist.Eq.
Correlation	0.957002	0.910564	0.92602	0.961689	-0.32491	-0.32265	0.209962	-0.45474	0.805717

data set is created by transforming the matrices formed in 50×50 Real Part and 50×50 Imag Part into vector matrix. Then, they are normalized and saved as datasets on the NN output side as the images of the motor geometry.

TABLE 5. MAPE (mean absolute percentage error) for NNs.

Group	Direct			Histogram			Feature Extraction		
NNs	SNNG	FFTRI	FFTMA	SNNG	FFTRI	FFTMA	SNNG	FFTRI	FFTMA
MAPE	1.28272	0.19415	0.02289	2.11827	0.06388	0.02282	7.26008E-06	5.78586E-06	9.08431E-06

TABLE 6. Testing data of the methodology.

Input Parameters for NNs	Training Data Best Result	Testing Data		
	From exp_18	1	2	3
Efficiency [%]	91.3014	90.0000	91.0000	92.0000
Rated Torque [Nm]	1.4645	1.4500	1.4600	1.4700
Stator Tooth Flux Density [Tesla]	1.2511	1.2400	1.2500	1.2600
Stator Yoke Flux Density [Tesla]	1.2195	1.2100	1.2200	1.2300
Rotor Top-Tooth Flux Density [Tesla]	0.6613	0.6400	0.6500	0.6600
Rotor Yoke Flux Density [Tesla]	0.7478	0.7400	0.7500	0.7600
Magnet Flux Density [Tesla]	0.9074	0.8900	0.9000	0.9100
Air-Gap Flux Density [Tesla]	0.3515	0.3400	0.3500	0.3600

FIGURE 5. Generated motor geometries from nns according to testing data.

TABLE 7. Generated motor features from the generated motor geometries according to testing data.

Test No	SOD	SID	ROD	RID	R_MT	R_MW	S_HS0	S_HS1	S_HS2	S_BS0	S_BS1	S_BS2	R_D1	R_O1	R_O2	R_B1	R_RIB	R_HRIB
1	120.34	74.34	73.26	22.1	3	26.44	0.64	0.68	8.93	1.6	7.55	10.12	72.28	2.14	3.08	4.71	2.17	4.06
2	120.94	74.19	73.18	22.83	3.38	25.9	0.65	0.61	8.28	1.83	7.6	10.01	72.15	2.11	3.17	4.78	2.15	4.02
3	121.2	75.34	74.25	21.68	3.57	25.16	0.64	0.68	8.48	1.51	7.43	9.99	72.33	2.25	3.19	4.52	2.18	3.95

6) TRAINING DATASET PREPARATION—4

Similar to the previous step, 50×50 matrices are decomposed with FFT. As a result of the decompose process, a 2500 × 1 data set is created by transforming the matrices formed in 50×50 Mag Part and 50×50 Angle Part into vector matrix. Then, they are normalized and saved as datasets on the NN output side as the images of the motor geometry.

7) TRAINING DATASET PREPARATION—5

Stator Outer Diameter SOD and Stator Inner Diameter SID, Stator Slot S_HS0, Stator Slot S_HS1, Stator Slot S_HS2, Stator Slot S_BS0, Stator Slot S_BS1, Stator Slot S_BS2, Rotor Outer ROD and Inner Diameter RID, Rotor R_D1, Rotor R_O1, Rotor R_O2, Rotor R_B1, Rotor R_RIB is Rotor R_HRIB, Magnet Thickness R_MT and Width R_MW parameters produced in Motor Design Parameters for DoE are imported to Matlab©working environment and saved as data on the NN output.

### 8) NEURAL NETWORKS TRAINING OPERATION—1

The training processes with the datasets produced from Training Dataset Preparation -1 to 5 are carried out for SNNGs of SNNG, FFTRI Real Part, FFTRI Imag Part, FFTMA Mag Part and FFTMA Angle Part.

### 9) TRAINING DATASET PREPARATION—6

Output data from the trained SNNG NN directly, output data from FFTRI Real Part, FFTRI Imag Part, FFTMA Mag Part and FFTMA Angle Part NNs are passed and composed with IFFT process to Direct (Reshaping 2500 × 36), 2D Histogram (300 × 36), and Feature Extraction (6 × 36) operations are performed. Then, they are normalized and saved as data on the NN input as the images of the motor geometry.
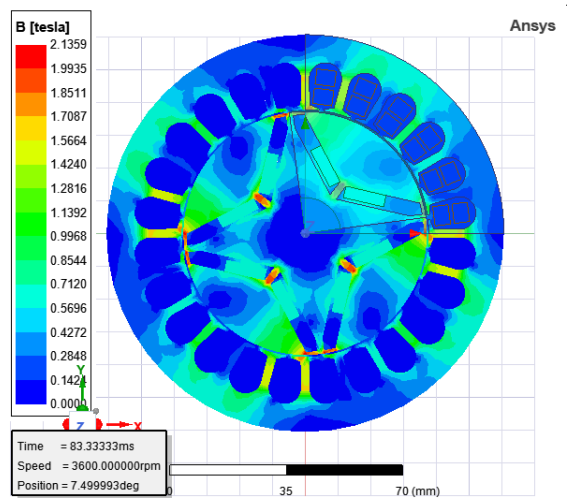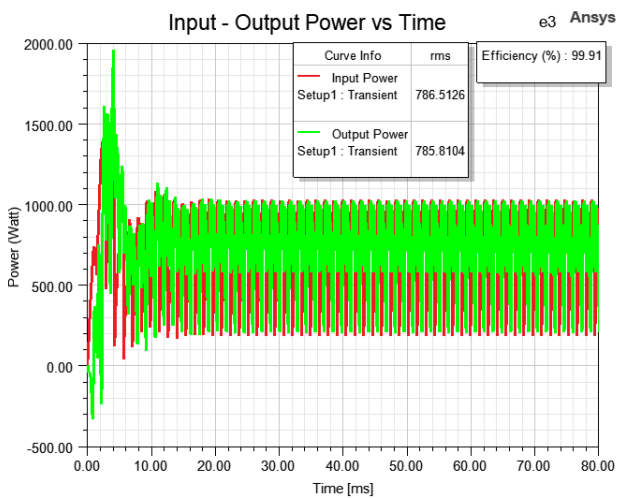
10) NEURAL NETWORKS TRAINING OPERATION—2

The training processes with the datasets produced from Training Dataset Preparation 1 to 5 are carried out for SNNG
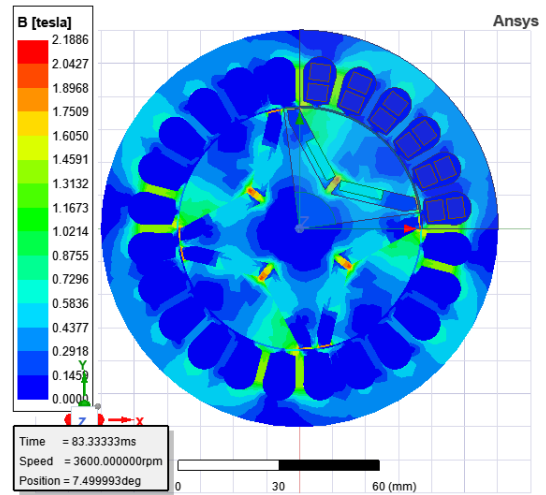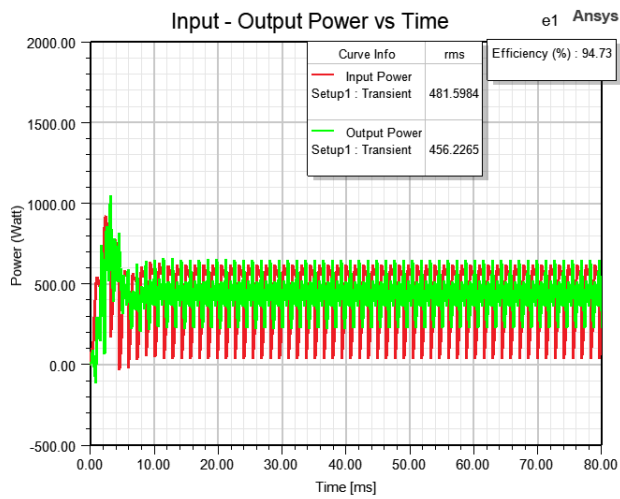
Ansys Maxwell 2D – IPM Model 1
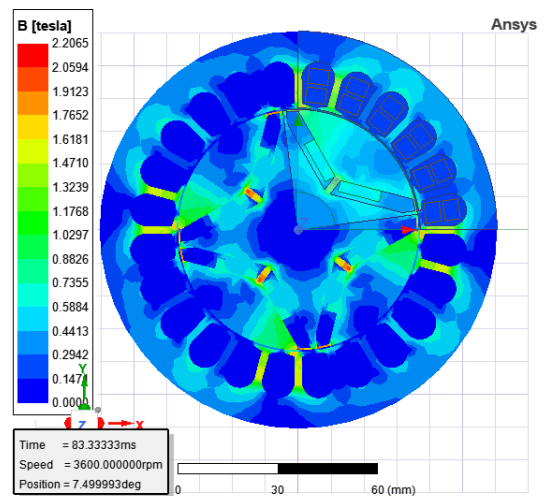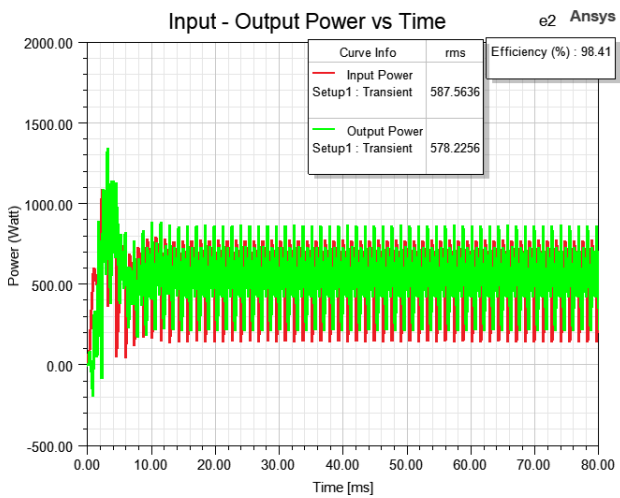
Ansys Maxwell 2D – IPM Model 2

Ansys Maxwell 2D – IPM Model 3

FIGURE 6. IPM performance results in ansys maxwell 2d according to Table 7.

TABLE 8. IPM performance results in ansys RMXprt according to Table 7.

Input Parameters for NNs	Testing IPM Model 1		Testing IPM Model 2		Testing IPM Model 3	
	Results	Error	Results	Error	Results	Error
Efficiency [%]	91.5862	1.73%	91.9099	0.99%	91.9249	0.08%
Rated Torque [Nm]	1.4641	0.96%	1.4696	0.65%	1.4534	1.14%
Stator Tooth Flux Density [Tesla]	1.1856	4.59%	1.2012	4.06%	0.9916	27.07%
Stator Yoke Flux Density [Tesla]	1.1813	2.43%	1.0124	20.51%	0.8275	48.64%
Rotor Top-Tooth Flux Density [Tesla]	0.4691	36.43%	0.4420	47.06%	0.4209	56.81%
Rotor Yoke Flux Density [Tesla]	0.5292	39.83%	0.5353	40.11%	0.5209	45.90%
Magnet Flux Density [Tesla]	0.9139	2.62%	0.9174	1.90%	0.9218	1.28%
Air-Gap Flux Density [Tesla]	0.3447	1.36%	0.3397	3.03%	0.2807	28.25%
	Average	11.24%	Average	14.79%	Average	26.15%
Error	Min.	0.96%	Min.	0.65%	Min.	0.08%
	Max.	39.83%	Max.	47.06%	Max.	56.81%

Direct, FFTRI Direct, FFTMA Direct, SNNG Histogram, FFTRI Histogram, FFTMA Histogram, SNNG Feat.Extrc., FFTRI Feat.Extrc. ve FFTMA Feat.Extrc.

IV. RESULTS AND DISCUSSION

During this study, a total of 14 neural networks (NNs) were utilized, with each NN having a similar structure but differing in the number of input and output ports. The NNs comprise an input port, output port, hidden layer, and output layer, with the parameter fitting being achieved through the manipulation of these layers.

The details of the NNs and their training performance results are given in Table 2. The activation functions used in the hidden and output layers during the parameter fitting process were tansig and pureline, respectively, as is commonly employed in such operations [64], [65]. The training algorithms used for the parameter fitting were Levenberg Marquardt and Scaled Conjugate Gradient, with the latter becoming necessary as the size of the input or output vector increases. Training algorithms such as Levenberg-Marquardt (Fast), Bayesian Regularization (Slow, Generalization Well), and Scaled Conjugate Gradient (Memory Efficient) are typically preferred for parameter fitting operations [65], [66]. Training was halted once the MSE and regression (R) values reached or exceeded the minimum regression value of 0.9.

A. TRAINING DATASET ANALYSIS

In this section, the trained networks are evaluated by considering the training datasets in L36. The L36 orthogonal test sequence is given in Table 3. Here, the parameters of the IPM used to create the datasets and the motor design parameter values corresponding to these levels are given. SOD, SID, ROD, RID, R_MT and R_MW given in Table 3 represent Stator Outer Diameter, Stator Inner Diameter, Rotor Outer Diameter, Rotor Inner Diameter, Rotor Magnet Thickness and Rotor Magnet Width, respectively. S_HS0, S_HS1, S_HS2, S_BS0, S_BS1, S_BS2, R_D1, R_O1, R_O2, R_B1,

R_RIB represent stator and rotor slot geometries. All data given in Table 3 are used in mm.

In Fig. 4, the motor models created in Ansys RMXprt using the data in Table 4 and subjected to gray scale and scaling processes in Matlab, and the image of the motor geometries derived from networks as a result of training are given. As can be seen in Table 4, the Log filter contributes to the improvement of the image by the best correlation result.

B. FEATURE EXTRACTION FROM THE GENERATED MOTOR GEOMETRY

In this section, the images of the motor geometries generated from SNNG, FFTRI and FFTMA NNs that provide the best results are evaluated. And the motor design parameters are obtained from the image of the motor geometry. Here, using 3 different algorithms (Direct (2500×56), Histogram (300×36) and Feature Extraction (6×36)) for 3 different NNs, the training of 9 NNs (SNNG Direct, FFTRI Direct, FFTMA Direct, SNNG Histogram, FFTRI Histogram, FFTMA Histogram, SNNG Feat.Extrc., FFTRI Feat.Extrc. and FFTMA Feat.Extrc.) are carried out. In the feature extraction process, 2D Maximum, 2D Mean, 2D Minimum, 2D Standard Deviation, 2D Variance and Histogram tools are used to create the input vector for NNs. The performance indicators obtained as a result of the training are given in Table 2 in terms of MSE and regression. As can be seen from the results here, the performance increased as input data size of the NN decreased. Similarly, the MAPE results for the motor design parameters in Table 5 show that the performance increases as input data size of the NN decreased

C. TESTING THE PROPOSED MODEL

As can be seen in Tables 4 and 5, SNNG gives the best performance in terms of the image of the motor geometry generation and FFTRI Feat.Extrc in terms of extracting motor design parameters. In order to reduce the processing, SNNG is chosen for the generation the image of the motor geometry

for testing, and SNNG Feat.Extrc is chosen for extracting the motor design parameters from the image geometry because SNNG Feat.Extrc provides the 2nd best performance in the estimation of motor design parameters. When the training data are analyzed, the parameters used as input data for the neural network test and their variations are given in Table 6. Here, the test combination that gives the best performance is processed. And with the changes in its percentile digit, test variations are created. The images of the motor geometry generated in the tests performed using the data in Table 6 and the design parameters of these motor are given in Fig. 5 and Table 7.

For the motor design parameters taken from Table 7, the obtained results for the 3 motor models created in Ansys RMXprt are given in Table 8. Similarly, the percentage error results obtained for the test data applied to the input of the neural networks in Table 6 are given in Table 8.

The results of the 2D finite element model (2D Ansys Maxwell) for the IPM models created using the Ansys RMXprt model are given in Fig. 6. Input and Output powers and RMS values for these analyzes are given for each IPM model in Fig. 6. The efficiency of the IPM models is calculated by RMS values. In addition, the results regarding the flux densities on the rotor, stator and slot geometries are given in Fig. 6. As it can be understood from Fig. 6, the obtained results with the empirical equations in Ansys RMXprt and the obtained results from the 2D Ansys Maxwell models are converge each other in terms of both efficiency and flux densities and confirmation of the model.

As a result of experiment and testing processes, the proposed model shows the satisfied results to generate the initial geometry image and extract the design parameters from image geometry of IPM motor. Furthermore, the generated geometry and extracted motor design parameters are met the desired performance requirements. Besides, the proposed method helps to extract the satisfied motor geometry and design parameters in one go and to prevent time wastage, despite the long computational processes of iterative optimization methods.

V. CONCLUSION

The process of selecting an initial model geometry, designing and verifying the motor, and conducting computer-aided analysis can be time-consuming and lead to reduced efficiency and higher costs. To improve this process, designers often focus on optimization techniques, including traditional design of experiment methods and artificial intelligence-based approaches. However, inappropriate initial model selection can prolong the optimization process. To address this challenge, a new approach that combines artificial intelligence and image processing is proposed in this study to improve the design, analysis, and optimization processes for motor designers. On the other hand, this approaches requires data preparation and training process for NN. Because the main problem on the optimization process is long FEM analysis, although the data preparation and training process are required, this approaches provide the simplification for the optimization process of e-motor by avoiding the iterative FEM analysis.

The proposed approach aims to generate motor geometries that meet specific design requirements using an artificial neural network. Different neural network structures are evaluated for their ability to generate motor geometries, and the learning rate of the artificial neural network is improved by decomposing and composing geometry images with FFT and IFFT. The neural networks are trained successfully using decomposing operation with FFT, which provides real-imaginary, magnitude-angle parts of the image geometry. However, the composition process with IFFT results in data loss due to float point situations, and the correlation coefficients of the generated geometries are not as similar as the learning success.

To improve the generated motor geometries, 2D filter techniques such as Log, FFT, Log+FFT, Laplacian, Sobel, and Histogram Equalization are applied. The Log filter is found to improve the motor geometry image. The dimension of the generated motor geometries is determined using feature extraction techniques such as Histogram, 2D Maximum, 2D Mean, 2D Minimum, 2D Standard Deviation, and 2D Variance to observe the neural network performance with different input vector dimensions. The results show that neural networks with small input vectors perform better and produce more successful results.

To validate the trained neural networks, three different requirement sets are created, and the trained neural networks and the IPM models in Fig. 5 are generated. The dimensional features of the generated IPM models are extracted using the trained neural networks, and the IPM design parameters in Table 7 are obtained. The performance of the neural networks is verified by modeling and analyzing the values in Table 7 in Ansys RMXprt, and the results in Table 8 are obtained. The neural network can generate models that meet efficiency and torque requirements with very high performance but flux densities with lower performance. Ansys RMXprt models are transformed into finite element models with Ansys Maxwell and analyzed, and similar results are obtained.

The proposed model is validated through analysis, and in future studies, the model will be trained with different topologies to generate solutions from a broader perspective.

REFERENCES

[1] C. Sun, T. Li, and X. Tang, "A data-driven approach for optimizing early-stage electric vehicle charging station placement," *IEEE Trans. Ind. Informat.*, early access, Feb. 16, 2023, doi: 10.1109/TII.2023.3245633.

[2] M. Ehsani, K. V. Singh, H. O. Bansal, and R. T. Mehrjardi, "State of the art and trends in electric and hybrid electric vehicles," *Proc. IEEE*, vol. 109, no. 6, pp. 967–984, Jun. 2021, doi: 10.1109/JPROC.2021.3072788.

[3] K. K. Prasad and V. Agarwal, "A comprehensive analysis of single-stage wireless power transfer compensation topologies for battery chargers in electric vehicles," in *Proc. IEEE Texas Power Energy Conf. (TPEC)*, College Station, TX, USA, Feb. 2020, pp. 1–6, doi: 10.1109/TPEC48276.2020.9042556.

[4] D. S. Yadav and M. Manisha, "Electric propulsion motors: A comparative review for electric and hybrid electric vehicles," in *Proc. IEEE Int. Conf. Distrib. Comput. Electr. Circuits Electron. (ICDCECE)*, Ballari, India, Apr. 2022, pp. 1–6, doi: 10.1109/ICDCECE53908.2022.9793099.

[5] X. Sun, Z. Shi, G. Lei, Y. Guo, and J. Zhu, "Multi-objective design optimization of an IPMSM based on multilevel strategy," *IEEE Trans. Ind. Electron.*, vol. 68, no. 1, pp. 139–148, Jan. 2021, doi: 10.1109/TIE.2020.2965463.

[6] L. Qin, X. Huang, and Y. Wang, "Research on electric vehicle DC speed regulation based on PSO optimization," in *Proc. 5th World Conf. Mech. Eng. Intell. Manuf. (WCMEIM)*, Ma'anshan, China, Nov. 2022, pp. 156–163, doi: 10.1109/WCMEIM56910.2022.10021425.

[7] Z. Wu, Z. Wang, and J. Zhang, "Research on parameter matching and optimization of hybrid electric vehicle power system," in *Proc. Int. Conf. Electr., Control Inf. Technol. (ECITech)*, Kunming, China, 2022, pp. 1–6.

[8] S. Wu, X. Huang, C. Tian, and P. Zhang, "Multi-physical field optimization analysis of high-speed permanent magnet synchronous motor based on NSGA-II algorithm," in *Proc. 22nd Int. Conf. Electr. Mach. Syst. (ICEMS)*, Harbin, China, Aug. 2019, pp. 1–6, doi: 10.1109/ICEMS.2019.8922236.

[9] X. Yi, C. Zhu, C. Huang, D. Wang, and X. Wang, "Design optimization of linear switched reluctance motor with segmental mover," in *Proc. 13th Int. Symp. Linear Drives Ind. Appl. (LDIA)*, Wuhan, China, Jul. 2021, pp. 1–6, doi: 10.1109/LDIA49489.2021.9505921.

[10] X. Zhao, Z. Sun, and Y. Xu, "Multi-objective optimization design of permanent magnet synchronous motor based on genetic algorithm," in *Proc. 2nd Int. Conf. Mach. Learn., Big Data Bus. Intell. (MLBDBI)*, Taiyuan, China, Oct. 2020, pp. 405–409, doi: 10.1109/MLBDBI51377.2020.00086.

[11] M. Staackmann, B. Y. Liaw, and D. Y. Y. Yun, "Dynamic driving cycle analyses using electric vehicle time-series data," in *Proc. 32nd Intersociety Energy Convers. Eng. Conf. (IECEC)*, Honolulu, HI, USA, 1997, pp. 2014–2018, doi: 10.1109/IECEC.1997.656736.

[12] S. M. Naylor, V. Pickert, and D. J. Atkinson, "Fuel cell drive train systems—Driving cycle evaluation of potential topologies," in *Proc. IEEE Vehicle Power Propuls. Conf.*, Windsor, U.K., Sep. 2006, pp. 1–6, doi: 10.1109/VPPC.2006.364368.

[13] J. Fan, C. Zhang, Z. Wang, Y. Dong, C. E. Nino, A. R. Tariq, and E. G. Strangas, "Thermal analysis of permanent magnet motor for the electric vehicle application considering driving duty cycle," *IEEE Trans. Magn.*, vol. 46, no. 6, pp. 2493–2496, Jun. 2010, doi: 10.1109/TMAG.2010.2042043.

[14] L. Chu, J. Yin, L. Yao, and W. Wang, "The method for matching the PMSM's base parameters of the hybrid electric vehicle based on drive cycle," in *Proc. Int. Conf. Electron Mech. Eng. Inf. Technol.*, Harbin, China, Aug. 2011, pp. 3234–3237, doi: 10.1109/EMEIT.2011.6023774.

[15] L. Jun, W. Wenbin, L. Gang, and L. Fangjun, "Simulation and emission experiment of Changan hybrid electric vehicle (HEV) under the instable drive cycle conditions," in *Proc. Int. Conf. Electr. Inf. Control Eng.*, Wuhan, China, Apr. 2011, pp. 2578–2581, doi: 10.1109/ICEICE.2011.5776913.

[16] R. Rothe and K. Hameyer, "Life expectancy calculation for electric vehicle traction motors regarding dynamic temperature and driving cycles," in *Proc. IEEE Int. Electric Mach. Drives Conf. (IEMDC)*, Niagara Falls, ON, Canada, May 2011, pp. 1306–1309, doi: 10.1109/IEMDC.2011.5994793.

[17] P. Juris, A. Brune, and B. Ponick, "A coupled thermal-electromagnetic energy consumption calculation for an electric vehicle with wheel hub drive considering different driving cycles," in *Proc. IEEE Vehicle Power Propuls. Conf.*, Seoul, South Korea, Oct. 2012, pp. 28–31, doi: 10.1109/VPPC.2012.6422655.

[18] L. Chen, J. Wang, P. Lazari, and X. Chen, "Optimizations of a permanent magnet machine targeting different driving cycles for electric vehicles," in *Proc. Int. Electr. Mach. Drives Conf.*, Chicago, IL, USA, May 2013, pp. 855–862, doi: 10.1109/IEMDC.2013.6556198.

[19] X. Wu, T. Jiang, J. Du, and C. Hu, "Comparison of different driving cycles control effects of an extended-range electric bus," in *Proc. 2nd Int. Conf. Meas., Inf. Control*, Harbin, China, Aug. 2013, pp. 1073–1076, doi: 10.1109/MIC.2013.6758145.

[20] M. A. Lintern, C. Walsh, S. Carroll, and R. Chen, "Simulation study on the measured difference in fuel consumption between real-world driving and ECE-15 of a hybrid electric vehicle," in *Proc. Hybrid Electr. Vehicles Conf. (HEVC)*, London, U.K., 2013, pp. 1–6, doi: 10.1049/cp.2013.1918.

[21] S. Sridharan and P. T. Krein, "Induction motor drive design for traction application based on drive-cycle energy minimization," in *Proc. IEEE Appl. Power Electron. Conf. Expo. (APEC)*, Fort Worth, TX, USA, Mar. 2014, pp. 1517–1521, doi: 10.1109/APEC.2014.6803508.

[22] Y. Wang, W. Zhu, and U. Schaefer, "Study on the real time driving cycles and its influence on design of the electrical motor of EV," in *Proc. IEEE Conf. Expo Transp. Electrific. Asia–Pacific (ITEC Asia–Pacific)*, Beijing, China, Aug. 2014, pp. 1–6, doi: 10.1109/ITEC-AP.2014.6940810.

[23] V. I. Patel, J. Wang, X. Chen, and W. Wang, "Thermal design and analysis of 6-phase fractional slot permanent magnet machines considering driving cycles," in *Proc. 7th IET Int. Conf. Power Electron., Mach. Drives (PEMD)*, Manchester, U.K., 2014, pp. 1–6, doi: 10.1049/cp.2014.0286.

[24] S. Gunther, S. Ulbrich, and W. Hofmann, "Driving cycle-based design optimization of interior permanent magnet synchronous motor drives for electric vehicle application," in *Proc. Int. Symp. Power Electron., Electr. Drives, Autom. Motion*, Ischia, Italy, Jun. 2014, pp. 25–30, doi: 10.1109/SPEEDAM.2014.6872108.

[25] V. Boscaino and R. Miceli, "Analysis of driving cycles effects on power supply requirements of a fuel cell powered light-weight electric vehicle," in *Proc. IEEE Int. Electric. Drives Conf. (IEMDC)*, Coeur d'Alene, ID, USA, May 2015, pp. 853–859, doi: 10.1109/IEMDC.2015.7409160.

[26] E. A. Grunditz and T. Thiringer, "Characterizing BEV powertrain energy consumption, efficiency, and range during official and drive cycles from gothenburg, Sweden," *IEEE Trans. Veh. Technol.*, vol. 65, no. 6, pp. 3964–3980, Jun. 2016, doi: 10.1109/TVT.2015.2492239.

[27] E. Carraro, M. Morandin, and N. Bianchi, "Traction PMASR motor optimization according to a given driving cycle," *IEEE Trans. Ind. Appl.*, vol. 52, no. 1, pp. 209–216, Jan. 2016, doi: 10.1109/TIA.2015.2477479.

[28] F. Guo and F. Zhang, "A study of driving cycle for electric cars on Beijing urban and suburban roads," in *Proc. IEEE Int. Conf. Power Renew. Energy (ICPRE)*, Shanghai, China, Oct. 2016, pp. 319–322, doi: 10.1109/ICPRE.2016.7871224.

[29] N. Degrenne and S. Mollov, "Real-life vs. standard driving cycles and implications on EV power electronic reliability," in *Proc. 42nd Annu. Conf. IEEE Ind. Electron. Soc. (IECON)*, Florence, Italy, Oct. 2016, pp. 2177–2182, doi: 10.1109/IECON.2016.7793633.

[30] Q. Li, T. Fan, X. Wen, Y. Li, Z. Wang, and J. Guo, "Design optimization of interior permanent magnet sychronous machines for traction application over a given driving cycle," in *Proc. 43rd Annu. Conf. IEEE Ind. Electron. Soc. (IECON)*, Beijing, China, Oct. 2017, pp. 1900–1904, doi: 10.1109/IECON.2017.8216321.

[31] M. Kitzberger, G. Bramerdorfer, S. Silber, H. Mitterhofer, and W. Amrhein, "Influence of hysteresis and eddy current losses on electric drive energy balance in driving cycle operation," in *Proc. 8th Int. Electric Drives Prod. Conf. (EDPC)*, Schweinfurt, Germany, Dec. 2018, pp. 1–7, doi: 10.1109/EDPC.2018.8658302.

[32] A. Charadsuksawat, Y. Laoonual, and N. Chollacoop, "Comparative study of hybrid electric vehicle and conventional vehicle under new European driving cycle and Bangkok driving cycle," in *Proc. IEEE Transp. Electrific. Conf. Expo, Asia–Pacific (ITEC Asia–Pacific)*, Bangkok, Thailand, Jun. 2018, pp. 1–6, doi: 10.1109/ITEC-AP.2018.8432599.

[33] D. Tan, H. Xue, K. Yang, A. Li, and H. Wang, "Study on the thermal characteristics of in-wheel motor drive system based on driving cycles," *IEEE Access*, vol. 7, pp. 14463–14471, 2019, doi: 10.1109/ACCESS.2018.2887143.

[34] L. Tian, L. Wu, X. Huang, and Y. Fang, "Driving range parametric analysis of electric vehicles driven by interior permanent magnet motors considering driving cycles," *CES Trans. Electr. Mach. Syst.*, vol. 3, no. 4, pp. 377–381, Dec. 2019, doi: 10.30941/CESTEMS.2019.00049.

[35] S. Lekshmi and P. S. Lal Priya, "Range extension of electric vehicles with independently driven front and rear PMSM drives by optimal driving and braking torque distribution," in *Proc. IEEE Int. Conf. Power Electron., Smart Grid Renew. Energy (PESGRE)*, Cochin, India, Jan. 2020, pp. 1–6, doi: 10.1109/PESGRE45664.2020.9070246.

[36] S. Vignesh, Y. K. Bhateshvar, M. R. B. Agrewale, and K. C. Vora, "Significance of driving cycle on performance parameters and range in small electric vehicle," in *Proc. IEEE 1st Int. Conf. Smart Technol. Power, Energy Control (STPEC)*, Nagpur, India, Sep. 2020, pp. 1–5, doi: 10.1109/STPEC49749.2020.9297781.

[37] X. Sun, Z. Shi, G. Lei, Y. Guo, and J. Zhu, "Multi-objective design optimization of an IPMSM based on multilevel strategy," *IEEE Trans. Ind. Electron.*, vol. 68, no. 1, pp. 139–148, Jan. 2021, doi: 10.1109/TIE.2020.2965463.

[38] T. V. Sarathkumar, M. Poornanand, and A. K. Goswami, "Modelling and simulation of electric vehicle drive through SAEJ227 & EUDC cycles," in *Proc. IEEE Students Conf. Eng. Syst. (SCES)*, Prayagraj, India, Jul. 2020, pp. 1–5, doi: 10.1109/SCES50439.2020.9236717.

[39] K. Diao, X. Sun, G. Lei, G. Bramerdorfer, Y. Guo, and J. Zhu, "System-level robust design optimization of a switched reluctance motor drive system considering multiple driving cycles," *IEEE Trans. Energy Convers.*, vol. 36, no. 1, pp. 348–357, Mar. 2021, doi: 10.1109/TEC.2020.3009408.

[40] M. Bagheri, E. Farjah, and T. Ghanbari, "Selective utilized phase number of multiphase induction motors strategy to enhance electric vehicles' drive range," in *Proc. 12th Power Electron., Drive Syst., Technol. Conf. (PEDSTC)*, Tabriz, Iran, Feb. 2021, pp. 1–5, doi: 10.1109/PEDSTC52094.2021.9405866.

[41] H. Sawada, R. Suzuki, Y. Okamoto, and S. Wakao, "Optimization of rotor structure for synchronous reluctance motor using coupled topology optimization based on electromagnetic field analysis and structural mechanics," in *Proc. 19th Int. Symp. Electromagn. Fields Mechatronics, Electr. Electron. Eng. (ISEF)*, Nancy, France, Aug. 2019, pp. 1–2, doi: 10.1109/ISEF45929.2019.9097069.

[42] H. Sasaki and H. Igarashi, "Topology optimization accelerated by deep learning," *IEEE Trans. Magn.*, vol. 55, no. 6, pp. 1–5, Jun. 2019, doi: 10.1109/TMAG.2019.2901906.

[43] S. Doi, H. Sasaki, and H. Igarashi, "Multi-objective topology optimization of rotating machines using deep learning," *IEEE Trans. Magn.*, vol. 55, no. 6, pp. 1–5, Jun. 2019, doi: 10.1109/TMAG.2019.2899934.

[44] X. Li, Y. Qi, T. Zhao, Y. Liu, L. Zhang, H. Xu, W. Yu, X. Zhao, and C. Zhang, "Data-driven deep reinforcement learning control: Application to new energy aircraft PMSM," in *Proc. China Autom. Congr. (CAC)*, Beijing, China, Oct. 2021, pp. 7132–7172, doi: 10.1109/CAC53003.2021.9728191.

[45] W. Wang, F. Qu, and W. Li, "Research on drive mode of hybrid powertrain based on lever method," in *Proc. IEEE 5th Adv. Inf. Manage., Communicates, Electron. Autom. Control Conf. (IMCEC)*, Chongqing, China, Dec. 2022, pp. 330–334, doi: 10.1109/IMCEC55388.2022.10020066.

[46] D. C. D. Silva, L. Kefsi, and A. Sciarretta, "An analytical model to optimize the powertrain sizing of fuel cell hybrid electric vehicles," in *Proc. IEEE Vehicle Power Propuls. Conf. (VPPC)*, Merced, CA, USA, Nov. 2022, pp. 1–8, doi: 10.1109/VPPC55846.2022.10003436.

[47] R. T. Mehrjardi, N. F. Ershad, and M. Ehsani, "Transmotor-flywheel powertrain assisted by ultracapacitor," *IEEE Trans. Transport. Electrific.*, vol. 8, no. 3, pp. 3686–3695, Sep. 2022, doi: 10.1109/TTE.2022.3152793.

[48] N. F. Ershad, R. T. Mehrjardi, and M. Ehsani, "High-performance 4WD electric powertrain with flywheel kinetic energy recovery," *IEEE Trans. Power Electron.*, vol. 36, no. 1, pp. 772–784, Jan. 2021, doi: 10.1109/TPEL.2020.3004866.

[49] A. Krings and C. Monissen, "Review and trends in electric traction motors for battery electric and hybrid vehicles," in *Proc. Int. Conf. Electr. Mach. (ICEM)*, Gothenburg, Sweden, vol. 1, Aug. 2020, pp. 1807–1813, doi: 10.1109/ICEM49940.2020.9270946.

[50] A. A.-E. Abdallh, L. Vandenbossche, and L. Lastra, "Higher strength low loss electrical steels for improved design and performance of interior permanent magnet traction motors," in *Proc. 11th Int. Electric Drives Prod. Conf. (EDPC)*, Erlangen, Germany, Dec. 2021, pp. 1–5, doi: 10.1109/EDPC53547.2021.9684206.

[51] J. Wang, W. Geng, J. Guo, L. Li, and Z. Zhang, "Design and performance comparison of novel flux-concentrating IPM machines for power generation system application of extended-range electric vehicle," *IEEE Trans. Ind. Electron.*, vol. 70, no. 5, pp. 4450–4460, May 2023, doi: 10.1109/TIE.2022.3183341.

[52] M. E. Elsayed, O. M. Hebala, H. A. Ashour, and M. S. Hamad, "A comparative study of different electric vehicle MotorDrive systems under regenerative breaking operations," in *Proc. 31st Int. Conf. Comput. Theory Appl. (ICCTA)*, Alexandria, Egypt, Dec. 2021, pp. 104–111, doi: 10.1109/ICCTA54562.2021.9916634.

[53] L. Niu and M. Zhang, "The loss and efficiency analysis and research of interior permanent magnet synchronous motors for traction applications," *IEEE Access*, vol. 11, pp. 5538–5557, 2023, doi: 10.1109/ACCESS.2023.3237214.

[54] R. Xu and W. Tong, "Multi-objective hierarchical optimization of interior permanent magnet synchronous machines based on rotor surface modification," *CES Trans. Electr. Mach. Syst.*, vol. 6, no. 4, pp. 352–358, Dec. 2022, doi: 10.30941/CESTEMS.2022.00046.

[55] Z. Wang, X. Zhang, and Y. Guo, "Three-vector predictive current control for interior permanent magnet synchronous motor," in *Proc. IEEE Int. Conf. Predictive Control Electr. Drives Power Electron. (PRECEDE)*, Jinan, China, Nov. 2021, pp. 443–448, doi: 10.1109/PRECEDE51386.2021.9680998.

[56] M. Aslan, A. B. Özpolat, C. İşçi, F. Eroğlu, and A. M. Vural, "Design and modelling of internal permanent magnet motor," *Int. J. Energy Eng. Sci.*, vol. 5, no. 2, pp. 80–104, Oct. 2020.

[57] G. G. Kumar, S. K. Sahoo, and P. K. Meher, "50 years of FFT algorithms and applications," *Circuits, Syst., Signal Process.*, vol. 38, no. 12, pp. 5665–5698, May 2019, doi: 10.1007/s00034-019-01136-8.

[58] V. Voronin, S. Tokareva, E. Semenishchev, and S. Agaian, "Thermal image enhancement algorithm using local and global logarithmic transform histogram matching with spatial equalization," in *Proc. IEEE Southwest Symp. Image Anal. Interpretation (SSIAI)*, Las Vegas, NV, USA, Apr. 2018, pp. 5–8, doi: 10.1109/SSIAI.2018.8470344.

[59] C. Leracitano, A. Paviglianiti, N. Mammone, M. Versaci, E. Pasero, and F. C. Morabito, "SoCNNet: An optimized Sobel filter based convolutional neural network for SEM images classification of nanomaterials," in *Progresses in Artificial Intelligence and Neural Systems* (Smart Innovation, Systems and Technologies), vol. 184, A. Esposito, M. Faundez-Zanuy, F. Morabito, and E. Pasero, Eds. Singapore: Springer, May 2020, doi: 10.1007/978-981-15-5093-5_10.

[60] C. Tian, Q. Zhang, G. Sun, Z. Song, and S. Li, "FFT consolidated sparse and collaborative representation for image classification," *Arabian J. Sci. Eng.*, vol. 43, no. 2, pp. 741–758, Feb. 2018, doi: 10.1007/s13369-017-2696-7.

[61] R. M. Thanki and A. M. Kothori, *Digital Image Processing Using SCILAB*. Cham, Switzerland: Springer, May 2018, doi: 10.1007/978-3-319-89533-8.

[62] K. Bredies and D. Lorenz, *Mathematical Image Processing*. Cham, Switzerland: Birkhäuser, 2018, doi: 10.1007/978-3-030-01458-2.

[63] R. R. Isnanto, A. A. Zahra, A. L. Kurniawan, and I. P. Windasari, "Face recognition system using feature extraction method of 2-D Gabor wavelet filter bank and distance-based similarity measures," in *Proc. 7th Int. Conf. Informat. Comput. (ICIC)*, Denpasar, Indonesia, Dec. 2022, pp. 1–4, doi: 10.1109/ICIC56845.2022.10007016.

[64] C. Chang, P. Chen, T. Chou, I. Wang, B. Hudec, C. Chang, C. Tsai, T. Chang, and T. Hou, "Mitigating asymmetric nonlinear weight update effects in hardware neural network based on analog resistive synapse," *IEEE J. Emerg. Sel. Topics Circuits Syst.*, vol. 8, no. 1, pp. 116–124, Mar. 2018, doi: 10.1109/JETCAS.2017.2771529.

[65] T. M. Bafitlhile, Z. Li, and Q. Li, "Comparison of Levenberg Marquardt and conjugate gradient descent optimization methods for simulation of streamflow using artificial neural network," *Adv. Ecol. Environ. Res.*, vol. 3, no. 11, pp. 238–256, Nov. 2018.

[66] M. Kirisci, I. Demir, and N. Simsek, "Comparative analysis of neural networks in the diagnosis of emerging diseases based on COVID-19," *Konuralp J. Math.*, vol. 9, no. 2, pp. 324–331, Oct. 2021.
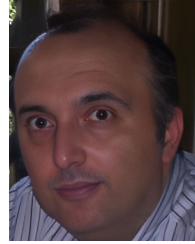
UGUR DEMIR received the Ph.D. degree in mechatronics engineering from Marmara University, in 2018. He is currently an Associate Professor with the Department of Mechatronics Engineering, Marmara University. He was involved in the development of novel electrical machine technologies for electric vehicle traction operations and mechatronics systems. His research interests include electromagnetic actuator design, design optimization of electrical machines, artificial neural network applications, autonomous driving, and advanced driving technologies.

GAZI AKGUN was born in Denizli, Turkey, in 1982. He received the B.Sc. degree in electrical education from Dicle University, Batman, Turkey, in 2004, and the M.Sc. and Ph.D. degrees in mechatronics engineering from Marmara University, Istanbul, in 2015 and 2019, respectively. From 2005 to 2021, he was a Vocational Technical Teacher in various cities around Turkey for the National Educational Ministry. He is currently an Assistant Professor with the Department of Mechatronics Engineering, Marmara University. His research interests include adaptive control, predictive control, and AI supported intelligent control systems, particularly in the fields of biomechatronics and rehabilitation robotics.

MUSTAFA CANER AKUNER received the Ph.D. degree in electrical education from Marmara University, in 1999. He is currently a Full Professor with the Department of Mechatronics Engineering, Marmara University. His research interests include electrical machines, battery electric vehicle, hybrid electric vehicle, and sustainable energy technologies.

OMER AKGUN received the first Ph.D. degree in communication engineering from Yildiz Technical University, in 2009, and the second Ph.D. degree from the Department of Electronic and Communication Education, Marmara University, in 2011. He is currently an Assistant Professor with the Department of Computer Engineering, Faculty of Technology, Marmara University. His current research interests include signal processing, biomedical signal processing, signal modeling, and communication systems.

TAHIR CETIN AKINCI (Senior Member, IEEE) received the bachelor's degree in electrical engineering, in 2000, and the master's and Ph.D. degrees, in 2005 and 2010, respectively. From 2003 to 2010, he was a Research Assistant with Marmara University, Istanbul, Turkey. Then, he became an Associate Professor with Istanbul Technical University (ITU) and held the position until 2021, after which he was promoted to a Full Professor with the Department of Electrical Engineering, ITU, in 2021. He assumed the role of a Visiting Scholar with the University of California, Riverside (UCR). His research interests include artificial neural networks, deep learning, machine learning, cognitive systems, signal processing, and data analysis. In 2022, he was honored with the International Young Scientist Excellence Award as well as the Best Researcher Award for his exceptional research achievements.

MAJID POURKARIMI received the B.Sc. degree in industrial engineering from Raja University, Iran, in 2004, and the M.Sc. degree in mechatronics engineering from Marmara University, in 2022. He is currently a PLM Industry Process Consultant with Dassault Systemes. His research interests include the design optimization of electrical machines, artificial neural network applications, and image processing.

• • •